ACS OMEGA

http://pubs.acs.org/journal/acsodf

Article

Molecular Dynamics Simulations of the Thermal Decomposition of 3,4-Bis(3-nitrofurazan-4-yl)furoxan

Yang Li, Yucun Liu,* Junming Yuan, Yiming Luo, Qiuli Jiang, Fanfan Wang, and Jingwei Meng

Cite This: *ACS Omega* 2021, 6, 33470−33481

Read Online

ACCESS | Metrics & More | Article Recommendations

ABSTRACT: When stimulated, for example, by a high temperature, the physical and chemical properties of energetic materials (EMs) may change, and, in turn, their overall performance is affected. Therefore, thermal stability is crucial for EMs, especially the thermal dynamic behavior. In the past decade, significant efforts have been made to study the thermal dynamic behavior of 3,4-bis(3-nitrofurazan-4-yl)furoxan (DNTF), one of the new high-energy-density materials (HEDMs). However, the thermal decomposition mechanism of DNTF is still not specific or comprehensive. In this study, the self-consistent-charge density-functional tight-binding method was combined with molecular dynamics (MD) simulations to reveal the differences in the thermal decomposition of DNTF under four heating conditions. The O−N (O) bond would fracture first during DNTF initial thermal decomposition at medium and low temperatures, thus triggering the cracking of the whole structure. At 2000 and 2500 K, NO_2 loss on outer ring I is the fastest initial thermal decomposition pathway, and it determines that the decomposition mechanism is different from that of a medium-low temperature. NO_2 is found to be the most active intermediate product; large molecular fragments, such as C_2N_2O, are found for the first time. Hopefully, these results could provide some insights into the decomposition mechanism of new HEDMs.

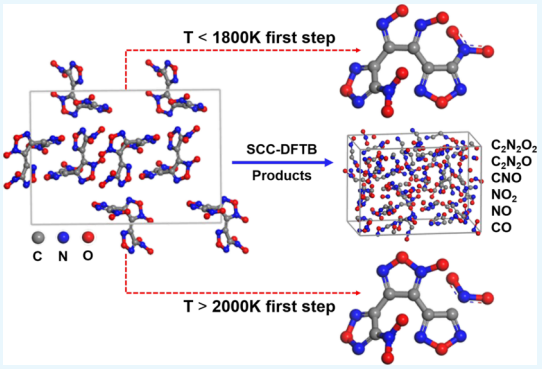

1. INTRODUCTION

Driven by military demands, developments in energetic materials (EMs) are progressing rapidly. New high-energy-density materials (HEDMs) with excellent performance, such as high density, high energy, high oxygen balance, and high thermal stability, are developed worldwide.[1] As a potential energetic component, the furazan ring has been designed and synthesized into a series of energetic compounds with excellent performance. 3,4-Bis(3-nitrofurazan-4-yl)furoxan (DNTF) is one of the most satisfactory furazan compounds in the research and application of new-generation HEDMs.

DNTF is an interesting molecule to study from both fundamental and applied perspectives. Since its first design and synthesis in the 1970s, only a handful of Russian scientists had information about DNTF in the following 35 years.[2] It was not until 2002 that the DNTF's synthetic route was first revealed; the crystal structure of DNTF was published in 2005.[3,4] DNTF has been the focus of many studies[5] ever since because of its unique structural configuration. The molecular structure of DNTF is composed of two furazan rings and one furoxan ring. The three five-member rings each form a plane structure. Each planar structure consists of two electrons of the C atom, two electrons of the N atom, and two lone pairs of electrons of the O atom, forming a conjugated pi bond.[6] This conjugated system bestows the structure with a high enthalpy of formation (657.23 kJ/mol), high oxygen balance, and increased stability.[7] However, the molecular structure of DNTF is not planar, and the spatial accumulation is in the shape of chairs. This unusual structure grants DNTF a dense crystal density (ρ = 1.937 g/cm^3) and a high detonation velocity (D = 9250 m/s).[8] With a low melting point (103−110 °C) and good melt-cast performance,[9] DNTF could form low eutectic systems with various EMs such as 2,4,6-trinitrotoluene (TNT), 1,3,3-trinitroazetidine (TNAZ), 2,4-dinitroanisole (DNAN), and octogen (HMX), which is expected to replace TNT as a candidate material for new-generation melt-cast explosive carriers.[10] Although the overall performance of DNTF is superior to that of HMX (ρ = 1.9 g/cm^3, D = 9000 m/s) and close to that of CL-20 (ρ = 2.04 g/cm^3, D = 9500 m/s),[11] its practical applications remain limited because of poor thermal safety. A large number of experimental studies have found that DNTF-based mixed explosives have high thermal sensitivity and cannot pass the cook-off test.[12−14] During the heating process, DNTF solid particles melt to form a local liquid-phase

Received: August 4, 2021
Accepted: November 15, 2021
Published: December 6, 2021

high-temperature region. Ignition reactions occur when the decomposition temperature is reached, and the growth rate is fast, due to which deflagration to detonation transition occurs easily.[15,16]

Energy and safety are the two most important properties of EMs, which depend on the thermodynamics and -kinetics of their decomposition, respectively.[17,18] However, there is often a contradiction between energy and safety, namely E&S contradiction, which is essentially a thermodynamics/-kinetics contradiction of EM decomposition. Energy is usually assessed by the detonation performance and safety by the degree to which EMs respond to external stimuli (e.g., sensitivity).[19] An ideal explosive would be one with a high performance but low sensitivity to satisfy the safety requirements. Therefore, the demand for new insensitive munition is increasing, and the thermodynamic and -kinetic behavior of new HEDM decomposition has gradually become a research hotspot.[20,21]

The study of the thermal decomposition reaction mechanism and kinetic behaviors can help better understand the structure−performance relationship and the mechanism of combustion explosion of HEDMs under heat.[22] Therefore, the thermal decomposition of DNTF has been studied a lot. Differential scanning calorimetry (DSC) is the most common experimental method to study the thermal decomposition of DNTF. The DSC curve reveals two stages in the thermal decomposition of DNTF,[23] the major exothermic peak at 292.41 °C and the second exothermic peak above 310 °C due to further decomposition of the decomposition products from the last stage in the condensed phase. With the increase of the pressure, the major exothermic peak moved in the high-temperature direction, and decomposition was intense; the second exothermic peak gradually became apparent.[24−26] Sinditskii et al.[27] proposed that the first stage of DNTF decomposition is the destruction of the furoxan ring, and the second one is the decomposition of the nitrofurazan fragment at higher temperatures; the main gaseous products identified with the fractional freezing method and FTIR spectroscopy are N_2O, CO_2, CO, NO_2, and an unknown polymer. Zhang et al.[28] innovatively utilized accelerating rate calorimetry to investigate the thermal decomposition of DNTF in a near adiabatic environment and found that the initial exothermic decomposition temperature was 180.7 °C, indicating a relatively high thermal stability.

The thermal decomposition of EMs is a complex process, which has been well studied at the macrolevel, but it is far from enough. The mechanism of microcosmic decomposition must be considered in order to achieve a comprehensive understanding of this process and to draw definite conclusions. Therefore, complex calculations are needed to help advance our understanding of chemical reactions.[29] In recent decades, the rapid development of quantum chemistry (QC) calculation methods and molecular dynamics (MD) simulation methods have profoundly impacted the development of EMs. In 2015, based on density functional theory (DFT), Tsyshevsky et al.[30] calculated activation barriers and reaction rate constants required by six possible decomposition channels of the DNTF gas-phase molecules and crystals (Figure 1), revealing that the elimination of the CN_2O_2 molecule via the outer ring cleavage (RC) (DM4 path, Figure 1) is the main reaction pathway for the DNTF decomposition in the gas phase; the DM4 path is still the predominant decomposition pathway at T < 1000 K for the DNTF solid-state decomposition, while the NO_2 loss (DM1, Figure 1) will be the fastest reaction at higher

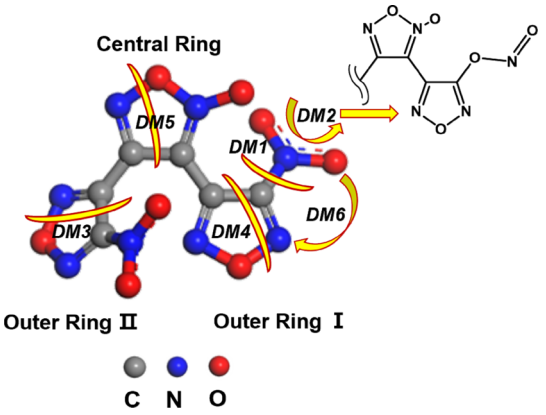

Figure 1. Six possible decomposition channels in DNTF.

temperatures. To some extent, CONO isomerization (DM2, Figure 1) may also influence the thermal decomposition of DNTF. The existence of the heterocyclic ring in the DNTF molecule determines that its initial thermal decomposition obviously differs from that of conventional nitro compounds. In addition, they showed that the thermal stability of DNTF is comparable to those of TATB and TNT, and the thermal sensitivity is lower than those of RDX, HMX, and PETN and comparable to or slightly higher than the benchmark sensitivity of TATB.[30]

The thermal decomposition process of EMs is usually dynamic, involving the change of temperature and pressure, as well as the interaction of multiple molecules and components, which cannot be fully revealed by QC calculations.[31] In addition, QC calculations hinder access to time scales (picoseconds to microseconds) relevant to thermodynamic transient reactions due to their high computational cost. Therefore, MD simulations are needed to supplement. MD simulations can not only reveal the influence of external factors (e.g., temperature and pressure) on the reaction process but also give the reaction path, primary and secondary reactions, and the distribution of each species over time. In contrast, first-principles molecular dynamics (QMD) simulation is a good choice for studying the thermodynamics and chemical reaction mechanism of condensed state EMs, which can be used to achieve both quantum-accuracy and simulate the reaction process on the scale of several tens of picoseconds.

Recently, Lindsey et al.[32] used the Mio + ChIMES approach, an effective machine learning (ML) method, to quickly tune density-functional tight-binding (DFTB) model to study the detonation chemistry of DNTF under extreme temperature (2000−9000 K) and pressure (5.5−35.6 GPa) conditions. They found that in DNTF decomposition, molecular products of CO_2, N_2, and CO were produced in abundance, and the system appears to reach metastable state earlier than other energetic materials with similar oxygen equilibrium (e.g., HMX). They also observed that the emergence and slow evolution of large $C_xN_yO_z$ species is a major feature of DNTF chemical changes under shock waves, and they are likely precursors of the carbon condensates observed in the experiments. Only more detailed MD simulations, larger on time and length scales than those accessible to DFTB, can draw more definitive conclusions.[32]

Although studies have been carried out on the thermal decomposition of DNTF in single-molecule gas-phase and condensed-state, they are not comprehensive. On the one

https://doi.org/10.1021/acsomega.1c04166
ACS Omega 2021, 6, 33470−33481

Table 1. Comparison of Experimental and Optimized Lattice Parameters of DNTF

lattice parameters	a, Å	b, Å	c, Å	α, deg	β, deg	γ, deg	density, g/cm^3	relative error, %
exp[3]	6.662	10.740	15.093	90	90	90	1.920	
opt (this work)	6.736	10.740	15.354	90	90	90	1.870	2.6
GGA-PBE-PAW[30]	7.028	11.212	15.634	90	90	90	1.683	10.2

hand, there is a lack of complete studies on the reaction process and product distribution over time in the thermal decomposition of DNTF, which changes dynamically with the influence of temperature. On the other hand, the temperature range tends to be polarized. In addition, the pyrolysis mechanism of EMs in the condensed phase is closer to the actual ignition and initiation process. To sum up, a comparative research of DNTF condensed-state dynamic thermal decomposition in a wide temperature range is necessary. This can not only complement and improve the thermal decomposition mechanism of DNTF but also contribute to a deep understanding of its sensitive mechanism.

Therefore, the self-consistent-charge DFTB (SCC-DFTB) method and MD simulations are used to explore the microthermal decomposition mechanism of DNTF at low and high temperatures and to reveal its reaction course and product distribution within the time scale accessible to MD simulations. The evolution processes of reactants, products, and potential energy (PE) with temperature are analyzed, and the pathways of initial thermal decomposition under different heating conditions are compared. The results show that heating conditions have a certain influence on the thermal decomposition mechanism of DNTF. Comparing the products under different heating conditions, it is found that high temperature is favorable to the formation of small molecular gas products. In addition to the common product molecular structure, larger molecular fragments such as C_2N_2O are also observed for the first time. Hopefully, these findings would contribute to understanding the structure−performance relationship of DNTF and provide valuable insights for predicting the properties of new HEDMs through MD simulations.

2. THEORETICAL CALCULATIONS

Thermal decomposition of DNTF was studied with the efficient approximate density functional theory, such as the density functional-based tight binding (DFTB) with the DFTB + source software package. DFTB+ has been successfully employed in studying EM applications as it enables simulations of large systems and large timescales with a reasonable accuracy while being considerably faster for typical simulations than the ab initio methods. The SCC-DFTB method is adopted to describe the charge fluctuations in the system as it offers a quantitative accuracy of the structural and energy parameters.[33,34]

MD simulations were conducted on DFTB+ 1.3.1 with the 3ob-2-1 parameter set,[35] and the SCC tolerance was set to 1.0 × 10^{-6} e. The *k*-points for the Brillouin-zone integration were specified as a 1 × 1 × 1 Monkhorst−Pack (MP) sampling. The Lennard-Jones dispersion model was used for dispersion correction.[36,37] Before MD simulations, the feasibility of the DFTB method needs to be verified. A conjugate gradient method was applied to relax the unit cell of DNTF. The maximum force component was set to 1.0 × 10^{-4} e. Comparing the optimized DNTF cell parameters of the SCC-DFTB method with those of the other DFT methods, the relative error with the experimental value is only 2.6% (Table 1), which is far lower than that of the GGA-PBE method, indicating the reliability of the SCC-DFTB method. Considering the computational time and resources of the MD simulations, a 2 × 2 × 1 supercell with 16 DNTF molecules or 352 atoms was built by repeating the unit cell. The unit cell of DNTF and the simulation models are shown in Figure 2.

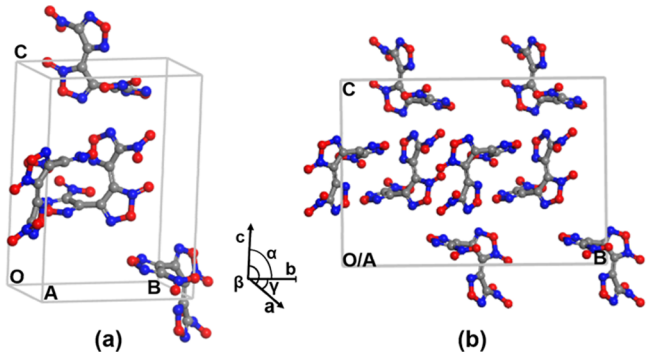

Figure 2. (a) Crystal structure of DNTF and (b) structure of the DNTF supercell.

Then, the MD simulations were performed using the NVT ensemble (constant number of atoms, constant volume, and constant temperature), and the temperature control was implemented with the Berendsen thermostat, at 300 K for 500 fs with a time step of 0.25 fs to release the stress in the DNTF supercell.[38−40] After that, MD simulations were carried out under four heating conditions, including constant temperature heating at 1800, 2000, and 2500 K and programed heating from 300 to 3000 K at a rate of 135 K/ps. Programed heating is similar to the cook-off test in practical application, while constant temperature heating at 1800, 2000, and 2500 K is selected in the hope of rapid energy exchange between the system and the external at relatively high temperatures, so that obvious initial reaction steps can be observed in a very short time (several tens of picoseconds). The time step of all simulations is 0.2 fs, and the total simulation time is 20 ps. The MD trajectories were recorded every 10 steps (2 fs). After the simulation, the FORTRAN program, written and provided by Zhang's team,[41−43] was used to analyze the evolution of PE, reaction path, and products in the MD process.

3. RESULTS AND DISCUSSION

3.1. Evolution of Potential Energy. PE is an important factor to describe the whole dynamic process as it determines the reaction activity at a given temperature. The increase of PE indicates that the reaction is in the endothermic stage, that is, the delay period or induction period in the thermal decomposition process of explosive. The PE drops and the reaction is in an exothermic stage, when the explosive begins to decompose rapidly.[39] Figure 3a illustrates the change of PE under programed heating from 300 to 3000 K. With the increase of the temperature, DNTF absorbs heat, causing a

https://doi.org/10.1021/acsomega.1c04166
ACS Omega 2021, 6, 33470−33481

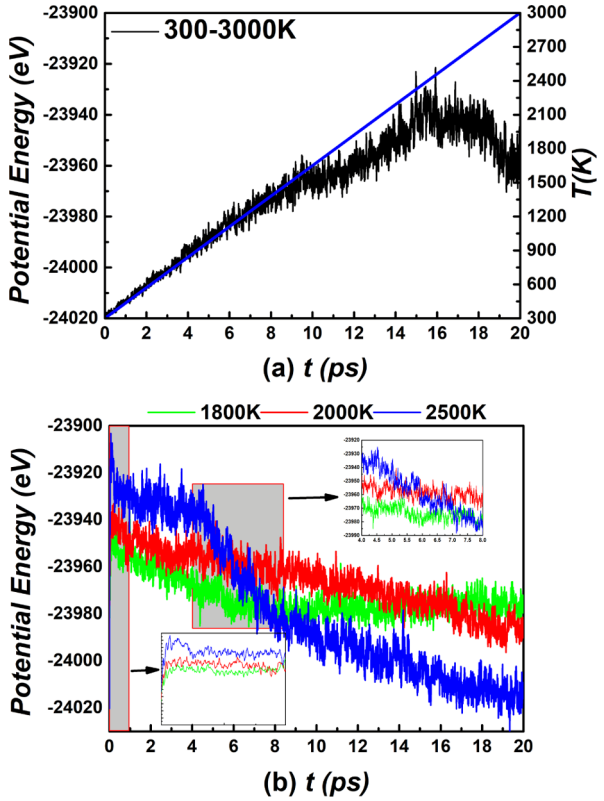

Figure 3. PE evolutions of DNTF under four heating conditions: (a) programed heating from 300 to 3000 K and (b) constant temperature heating at 1800, 2000, and 2500 K [the blue line in (a) represents the change of temperature with time, and the same curves in the following figures all follow this description].

gradual increase in PE, accompanied by a small amount of decomposition reaction. At ∼10 ps, T = 2000 K, the PE curve shows a turning point. At 10−15 ps, the PE changes slightly slowly, which was caused by the decomposition reaction gradually intensified with the increasing temperature. At ∼15 ps, T > 2000 K, PE peaked, and the violent decomposition reaction began. A large number of molecular fragments further broke down, and PE dropped gradually. However, decomposition is slow at 15−18 ps. At ∼18 ps, the temperature approached 2500 K, the decomposition rate accelerated, and the equilibrium was not reached at the end of the simulation time.

Figure 3b shows the evolution of PE at 1800, 2000, and 2500 K, respectively. PE peaked rapidly and then decreased. The higher the initial decomposition of PE, the higher the reaction activity at a given temperature.[44] As can be seen, the higher the temperature, the maximum value of PE is higher, and the higher PE causes the decomposition reaction much faster, as shown by the rapid reduction of PE. Before ∼4 ps, the decomposition rates at 1800, 2000, and 2500 K are almost the same. At 4−8 ps, the decomposition rates at 1800 and 2000 K are basically the same, while at 2500 K, the decomposition rates are obviously accelerated. At 8−20 ps, the PE curve at 1800 K tends to be stable first, and the rate at 2000 K remains unchanged, while the decomposition at 2500 K begins to slow down and is still faster than that at 2000 K. In general, the reaction activity is higher at 2500 K. Undoubtedly, the higher the temperature, the worse the thermal stability of DNTF.

3.2. Initial Thermal Decomposition of the DNTF Supercell. The FindMole procedure[45] was used in the FORTRAN script to process the data and analyze the initial dynamic decomposition trajectory of DNTF. In simulations, all DNTF molecules were cleaved in a unimolecular way during the initial thermal decomposition process. The results showed three types of initial thermal decomposition: (1) the ring-opening reaction caused by O−N bond fracture; (2) the ring-breaking reaction caused by C−C bond fracture; and (3) the NO_2 loss via C−NO_2 bond fracture. Among them, O−N and C−C bond fractures occurred on both the furazan ring and the furoxan ring. Therefore, the initial thermal decomposition is broken down into six types: (a) the fracture of the O−N bond on the furoxan ring; (b) the fracture of the O−N (O) bond on the furoxan ring; (c) the fracture of the O−N bond on the furazan ring; (d) the fracture of the C−C bond on the furoxan ring; (e) the fracture of the C−C bond on the furazan ring; and (f) the fracture of C−NO_2 bond (Figure 4). First, the reaction types and initial time of the first three steps of initial thermal decomposition under four heating conditions were statistically analyzed (Tables 2−4).

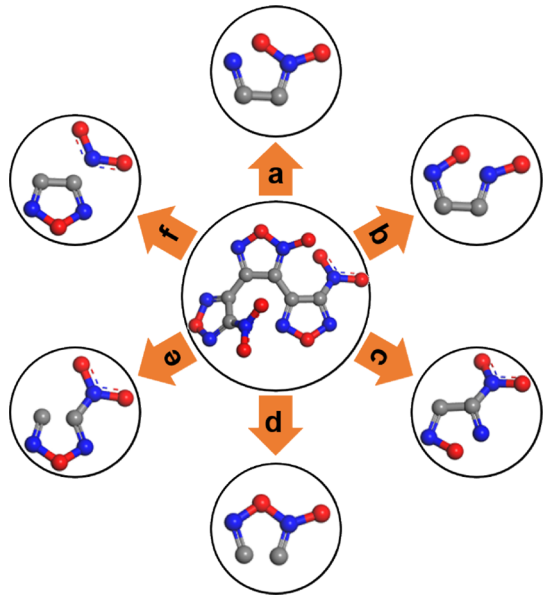

Figure 4. Six initial thermal decomposition types of the DNTF supercell: (a) fracture of the O−N bond on the furoxan ring, (b) fracture of the O−N (O) bond on the furoxan ring, (c) fracture of the O−N bond on the furazan ring, (d) fracture of the C−C bond on the furoxan ring, (e) fracture of C−C bond on the furazan ring, and (f) fracture of the C−NO_2 bond.

Tables showed that when T < 1000 K, only the (b) reaction took place and at the first step of initial thermal decomposition. With the increasing temperature, all kinds of reactions appeared to varying degrees in the following two steps. When T > 1300 K, the (f) reaction occurred. At 1800 K, the (b) reaction was still the first to occur. With the accumulation of heat, various reactions appeared in different degrees in the initial thermal decomposition process, and the proportion of the (f) reaction increased significantly. However, at 2000 and 2500 K, the (f) reaction occurred fastest, and at the third step of the initial thermal decomposition, the proportion of the (f) reaction is the largest at 2500 K. Therefore, we consider that when T < 1800 K, the O−N (O)

https://doi.org/10.1021/acsomega.1c04166
ACS Omega 2021, 6, 33470−33481

Table 2. Comparison of the Reaction Types and Initiation Time in the First Step of Initial Thermal Decomposition under the Four Heating Conditions

300−3000 K			1800 K		2000 K		2500 K	
T, K	reaction type	*t*, ps	reaction type	*t*, ps	reaction type	*t*, ps	reaction type	*t*, ps
432.81	b	3.206	b	0.102	f	0.014	f	0.008
814.32	b	6.032	b	0.110	c	0.016	c	0.012
857.25	b	6.350	b	0.126	c	0.040	f	0.020
914.22	b	6.772	f	0.148	c	0.042	c	0.022
945.81	b	7.006	b	0.162	b	0.074	b	0.022
959.58	b	7.108	c	0.188	f	0.126	f	0.022
970.92	b	7.192	f	0.208	f	0.154	f	0.024
997.38	b	7.388	a	0.218	f	0.194	b	0.040
1101.60	b	8.160	f	0.294	b	0.210	c	0.052
1169.64	c	8.664	b	0.334	c	0.210	f	0.070
1182.60	b	8.760	b	0.364	b	0.246	c	0.082
1206.09	b	8.934	b	0.510	c	0.380	b	0.154
1236.06	b	9.156	b	0.752	b	0.396	c	0.156
1279.26	c	9.476	b	0.958	b	0.404	b	0.176
1284.39	a	9.514	b	1.056	f	0.590	c	0.356
1285.20	a	9.520	c	1.254	b	2.234	b	1.202

Table 3. Comparison of the Reaction Types and Initiation Time in the Second Step of Initial Thermal Decomposition under the Four Heating Conditions

300−3000 K			1800 K		2000 K		2500 K	
T, K	reaction type	*t*, ps	reaction type	*t*, ps	reaction type	*t*, ps	reaction type	*t*, ps
1046.52	d	7.752	d	0.130	a	0.032	f	0.018
1075.68	c	7.968	d	0.170	e	0.090	d	0.038
1172.34	e	8.684	b	0.232	b	0.162	f	0.056
1207.98	d	8.948	e	0.250	e	0.168	d	0.056
1222.83	c	9.058	b	0.326	e	0.242	b	0.072
1279.26	c	9.476	c	0.364	c	0.306	f	0.098
1287.63	e	9.538	f	0.530	d	0.326	c	0.112
1315.17	c	9.742	b	0.676	f	0.408	b	0.116
1327.86	d	9.836	f	0.734	c	0.546	e	0.174
1328.94	c	9.844	d	0.936	f	0.678	d	0.176
1341.63	c	9.938	f	1.222	c	0.682	d	0.274
1342.44	c	9.944	e	1.280	c	0.696	b	0.374
1370.79	d	10.154	c	1.442	b	0.956	e	0.374
1382.40	c	10.240	c	1.762	b	1.464	c	0.63
1576.26	f	11.676	c	3.536	f	1.924	b	0.904
1576.53	c	11.678	f	4.126	f	3.208	d	1.220

bond on the furoxan ring is the key, which first occurs and triggers the decomposition of the entire DNTF molecule structure. When $T > 2000$ K, the fracture of the C−NO_2 bond is the fastest reaction. At the same time, it can also be seen that at 1800, 2000, and 2500 K, with the increase of temperature, the earlier the initial thermal decomposition started, the faster the reaction proceeded.

In order to more intuitively see the proportion changes of various reactions, the statistical data of reaction types in each step of initial thermal decomposition of the DNTF supercell under four heating conditions are shown in Figure 5. The MD results in the case of programed heating from 300 to 3000 K showed that the first step of the initial thermal decomposition was the ring-opening reaction caused by O−N bond fracture with the (b) reaction as the dominant reaction. In the second step, the (c) reaction was dominant. Due to the increase in temperature, some C−C bonds fractured. Among them, the (d) reaction was more frequent, and very few C−NO_2 bonds fractured. In the third step, the number of C−C bond fractures increased significantly, mainly manifested as the (e) reaction. There is also a slight increase in the (f) reaction.

As can be seen from the figure, at 1800, 2000, and 2500 K, the occurrence of the (a,b) reactions was inhibited due to the increase of the (f) reaction at the first step of the initial thermal decomposition with the increase of temperature; C−C bond fracture always starts to occur in the second step.

At 1800 K, the first step is still dominated by the (b) reaction despite the occurrence of the (f) reaction. In the second step, the (c) reaction and (d) reaction were dominant in the ring-opening reaction caused by the N−O bond fracture and the ring-breaking reaction caused by C−C bond fracture, respectively; the proportion of the (f) reaction increased. In the third step, the C−C bond fracture was the main reaction, and the (d) reaction dominated; the proportion of the (f) reaction is the same. At 2000 and 2500 K, O−N bond fractures were still the main reaction in the first step, but the proportion of the (f) reaction was the same under the two temperature conditions. In the second step, at 2000 K, O−N bond fractures

https://doi.org/10.1021/acsomega.1c04166
ACS Omega 2021, 6, 33470−33481

Table 4. Comparison of the Reaction Types and Initiation Time in the Third Step of Initial Thermal Decomposition under the Four Heating Conditions

300−3000 K			1800 K		2000 K		2500 K	
T, K	reaction type	*t*, ps	reaction type	*t*, ps	reaction type	*t*, ps	reaction type	*t*, ps
1076.22	c	7.972	f	0.334	f	0.190	f	0.022
1156.68	e	8.568	d	0.360	e	0.196	f	0.068
1227.69	e	9.094	e	0.394	d	0.254	f	0.098
1267.92	b	9.392	d	0.970	e	0.324	d	0.112
1305.45	f	9.670	d	1.074	b	0.344	e	0.144
1320.30	e	9.780	c	1.092	e	0.454	e	0.182
1334.61	e	9.886	d	1.144	f	0.568	e	0.184
1348.11	e	9.986	f	1.328	b	0.598	c	0.192
1349.73	f	9.998	e	1.460	e	0.710	f	0.274
1357.56	f	10.056	f	1.586	b	0.714	b	0.456
1389.96	e	10.296	e	1.788	c	0.746	f	0.550
1476.90	c	10.940	c	1.914	d	1.506	d	0.570
1550.88	c	11.488	f	2.262	d	1.686	c	0.656
1582.20	e	11.720	e	3.568	c	2.060	f	0.708
1714.23	d	12.698	d	4.282	f	3.870	c	0.908
1782.27	c	13.202	d	5.036	d	4.716	f	1.438

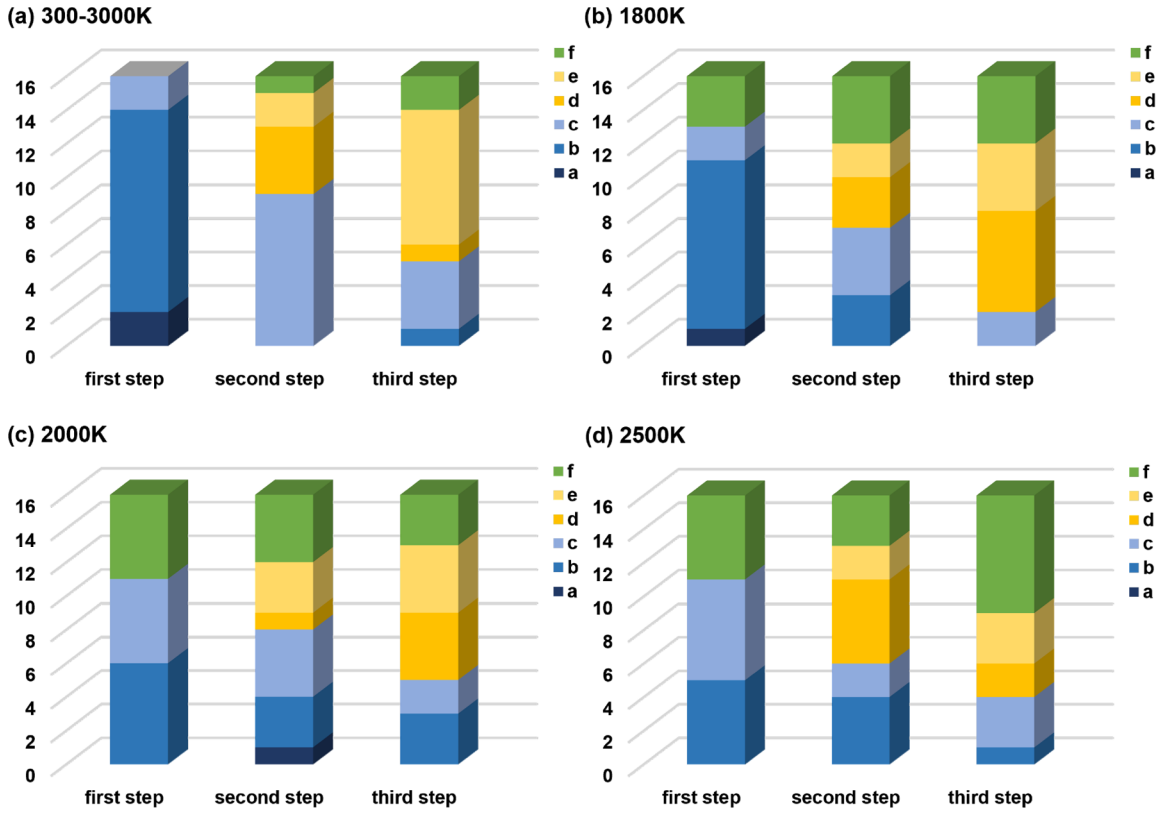

Figure 5. Number of molecules in the six decomposition types of the three DNTF supercells' initial thermal decomposition steps under the four heating conditions: (a) programed heating from 300 to 3000 K, (b) constant temperature heating at 1800 K, (c) constant temperature heating at 2000 K, and (d) constant temperature heating at 2500 K.

still occupied a large proportion, in which the (c) reaction was dominant; at 2500 K, the C−C bond fractures mostly, and the (d) reaction was the main reaction. In the third step, the C−C bond fracture increased significantly at 2000 K, while the (f) reaction's proportion decreased with time; however, the (f) reaction was dominant at 2500 K. Therefore, it can be found that when T < 1800 K, the O−N (O) bond breaking reaction on the furoxan ring not only takes place first but also is the most important reaction in the first step of the initial thermal decomposition of DNTF. The rupture of the C−C bond always lags behind that of the O−N bond or the C−NO_2 bond.

Combined with the above tables and figures and the animations of DNTF thermal decomposition, the main initial thermal decomposition pathways under four heating conditions were obtained, as shown in Figure 6. Tsyshevsky et al.[30] calculated the activation barriers (E), zero-point energy corrected barriers (E_{ZPE}), and pre-exponential factors (log A)

https://doi.org/10.1021/acsomega.1c04166
ACS Omega 2021, 6, 33470−33481

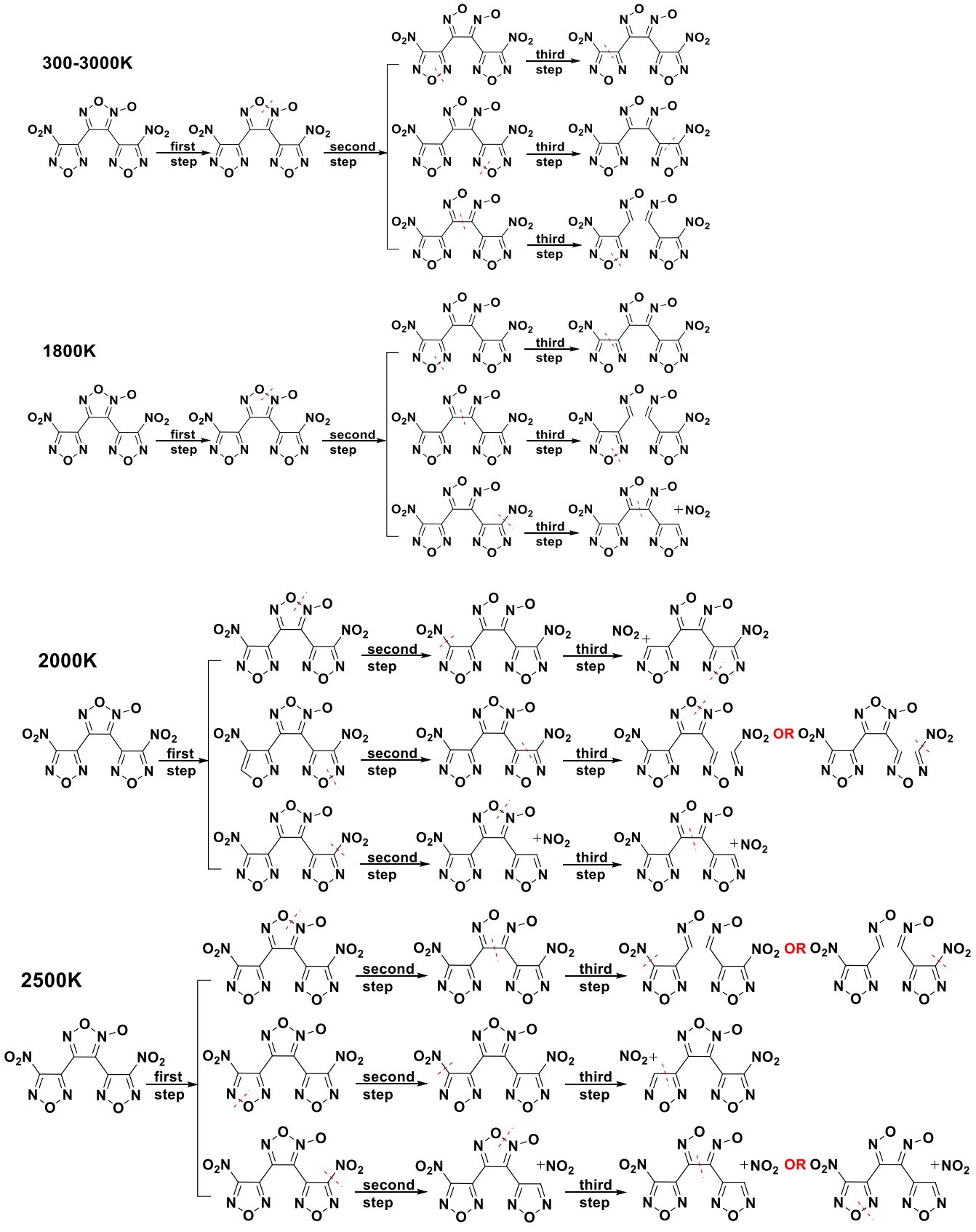

Figure 6. Main initial thermal decomposition pathways of the DNTF supercell under the four heating conditions.

of each possible thermal decomposition path of DNTF (Figure 1), as shown in Table 5. From the gas-phase data, they obtained four fast, low-energy reaction paths, which were also the paths that were focused on in the study of solid-state decomposition. As shown in Table 5, the paths correspond to the activation barrier value of solid-state decomposition. The

https://doi.org/10.1021/acsomega.1c04166
ACS Omega 2021, 6, 33470−33481

Table 5. Calculated Activation Barriers, Zero-Point Energy-Corrected Barriers, and Pre-Exponential Factors of DNTF Thermal Decomposition Reactions using the Hybrid PBE Functional[30]

		gas-phase decomposition			solid-state decomposition		
	reaction	E, kcal/mol	E_{ZPE}, kcal/mol	log A, s^{-1}	E, kcal/mol	E_{ZPE}, kcal/mol	log A, s^{-1}
DM1	NO_2 loss (I)	63.7	59.8	18.0	60.1	56.2	18.4
	NO_2 loss (II)	66.1	62.0	18.3			
DM2	CONO (I)	49.5	47.2	13.7	49.1	46.8	13.3
	CONO (II)	53.3	50.8	13.9			
DM3	RC (I) CN_2O_3	48.5	45.5	15.3	48.0	45.1	15.5
	RC (II) CN_2O_3	48.0	45.0	15.2			
DM4	RC (I) CN_2O_2	47.6	44.5	16.3	44.2	41.4	15.4
	RC (II) CN_2O_2	47.5	44.4	15.4			
DM5	RC (central ring)	61.8	59.1	14.6			
DM6	O-transfer (I)	71.0	68.7	13.3			
	O-transfer (II)	74.3	71.8	13.2			

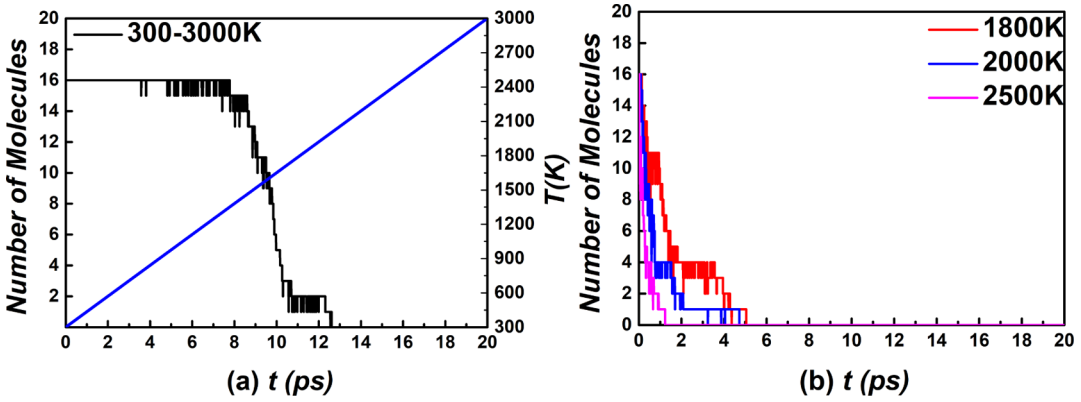

Figure 7. DNTF molecule evolutions under the four heating conditions: (a) programed heating from 300 to 3000 K and (b) constant temperature heating at 1800, 2000, and 2500 K.

outer ring I is more likely to decompose than the outer ring II. Figure 6 also reflects that most of the reactions occur in the outer ring I. The difference is that when T < 1000 K, the O−N (O) bond fracture [i.e., (b) reaction] is the main reaction on the central ring, rather than DM4 mentioned in the literature. This will be the result of the interaction between molecules, the spatial structure of the crystal, and the charge transfer. This needs to be studied using advanced QC or MD methods on a large scale but all need to be rigorously adapted to be useful for modeling EMs.[46] It is relatively difficult for the current research methods. However, there is no denying that this phenomenon has been observed. The similar situation also appeared in the studies of thermal decomposition of a similar structure to DNTF.[47,48]

It seems that the O−N (O) bond fracture requires a lower activation barrier than the outer ring cleavage, which is also the reason for DNTF's high sensitivity. Combined with the previous analysis, especially at 300−3000 K, the rupture of O−N (O) bond triggers the beginning of decomposition reaction, and the initial thermal decomposition is basically completed in the endothermic stage. Thus, when the temperature increases to the thermal decomposition temperature, a violent decomposition reaction will occur. This is why DNTF ignition is growing so fast.

In addition, the O−N bond fracture in the outer ring was always followed by the C−C bond fracture in the same ring because the cleavage of the outer ring always occurred under the concerted action of N−O and C−C bonds. When T > 2000 K, the C−NO_2 bond first breaks, which triggers the cleavage of the central ring in the same molecular structure, but inhibits the cleavage of outer rings due to its higher pre-exponential factor. This is attributed to the fact that the generation of NO_2 increases the number of molecules, thus enhancing the entropy effect of the system and changing the original decomposition law.[38] It is worth mentioning that no isomerization of CONO was found.

From the above discussion, we can know that the reaction activity of the system increases with the increase of temperature, and all kinds of reactions may occur, which is also the reason why the initial thermal decomposition pathway is not the only one. When T < 1800 K, the fracture of the O−N (O) bond on the furoxan ring is the key step affecting thermal decomposition. C−NO_2 bond breaks fastest at T > 2000 K and adds additional constraints to the thermal decomposition mechanism.

3.3. Evolution of Reactants and Products during DNTF Thermal Decomposition. The analysis of reactants and products contributes to understanding the thermal decomposition of EMs and the pyrolysis mechanism. The thermal decomposition evolution of DNTF molecules under the four heating conditions is shown in Figure 7. Figure 7a shows that before 8 ps, DNTF molecules basically remained unchanged, rapidly decreased at 8−10 ps, stabilized at 10−12 ps, and the number of DNTF molecules at ∼13 ps became zero. Because the ring-opening reaction in DNTF cannot be reflected in the quantity statistics, it is only shown after the ring-breaking or the NO_2 loss reaction. Therefore, no changes of DNTF molecules were observed before 8 ps, and at ∼13 ps,

https://doi.org/10.1021/acsomega.1c04166
ACS Omega 2021, 6, 33470−33481

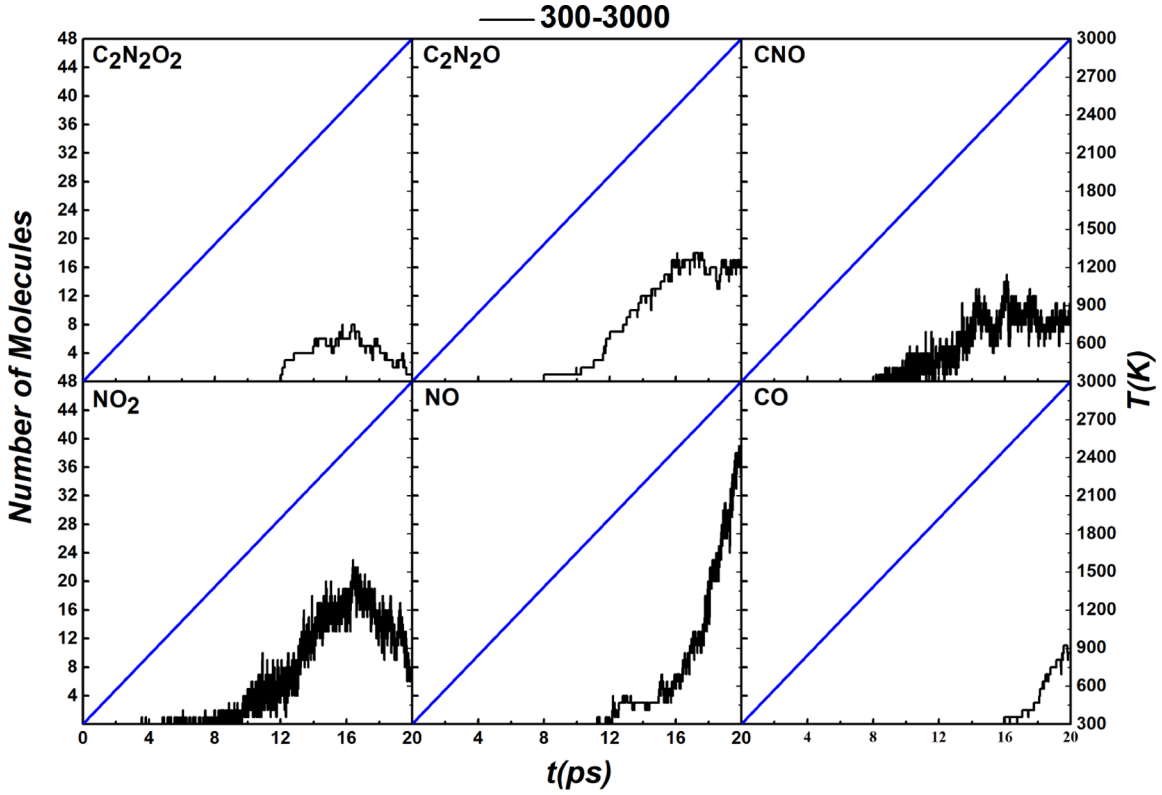

Figure 8. Evolutions of six products in the case of programed heating from 300 to 3000 K.

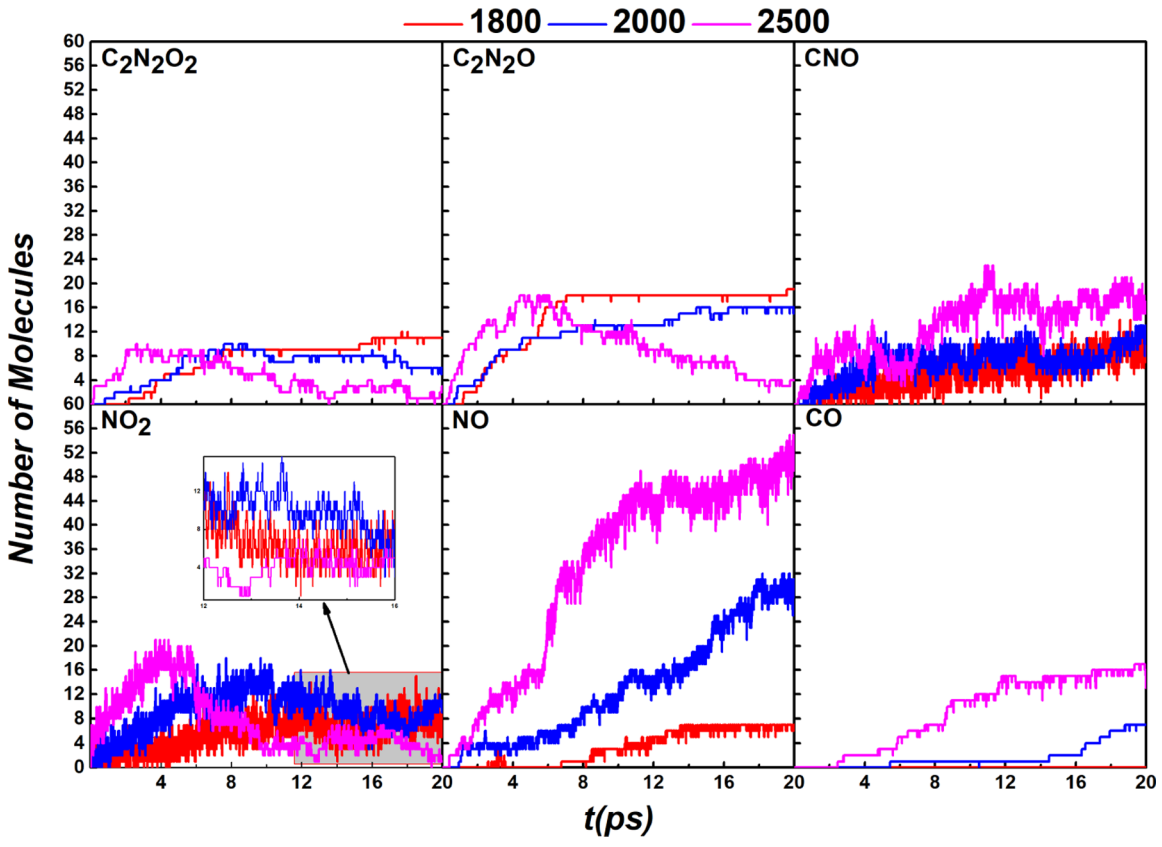

Figure 9. Evolutions of the six products under the three heating conditions.

all DNTF molecules underwent initial thermal decomposition, which was consistent with the time as shown in Tables 2 and 4.

As can be seen from Figure 7b, under the three constant-temperature heating conditions, the higher the temperature,

https://doi.org/10.1021/acsomega.1c04166
ACS Omega 2021, 6, 33470−33481

Table 6. Comparison of the Most Frequent Reactions and the Relative Molecular Mass of Products at the End of the Simulation Time under the Four Heating Conditions

			Products	
T, K	reaction	frequency	small molecular fragment ($M \leq 62$)	large molecule fragment ($M > 62$)
300−3000	$CN_2O_3 \Rightarrow CNO + NO_2$	15	86	26
	$NO_2 \Rightarrow O + NO$	14		
1800	$C_3N_4O_4 \Rightarrow C_2N_2O + CN_2O_3$	15	27	51
	$C_6N_8O_8 \Rightarrow C_3N_4O_4 + C_3N_4O_4$	10		
2000	$CN_2O_3 \Rightarrow CNO + NO_2$	12	68	32
	$NO_2 \Rightarrow O + NO$	9		
2500	$NO_2 \Rightarrow O + NO$	17	111	13
	$CN_2O_3 \Rightarrow CNO + NO_2$	8		

the faster the decomposition rate of DNTF, and the earliest the number of DNTF molecules tended to zero, the worse its thermal stability.

The six most frequently found products in DNTF thermal decomposition include $C_2N_2O_2$, C_2N_2O, CNO, NO_2, NO, and CO. Figure 8 illustrates the evolution of six products in the case of programed heating from 300 to 3000 K. After 8 ps, C_2N_2O, CNO, and NO_2 were found to increase. At ∼12 ps, $C_2N_2O_2$ and NO began to appear, while the number of DNTF molecules approached zero. At ∼16 ps, T > 2000 K, all the products except NO and CO reached the maximum value, NO began to rise sharply, and CO began to appear and continued to increase with the increase of temperature. At 16−20 ps, only $C_2N_2O_2$ and NO_2 began to decrease, so it can be seen that the further decomposition of $C_2N_2O_2$ and NO_2 is the reason for the increase of NO and CO.

Figure 9 shows the evolution of these products under constant heating at 1800, 2000, and 2500 K. The higher the temperature, the earlier the products appeared. At the end of the simulation time scale of 20 ps, more $C_2N_2O_2$ and C_2N_2O larger molecular fragments remained at 1800 K, and the emergence of NO was attributed to the decomposition of NO_2, while the emergence of CO was not observed, indicating that compounds containing C and O elements did not decompose further into stable small molecular gas products. This is because the temperature of further DNTF decomposition is higher than 1800 K. At 2000 K, $C_2N_2O_2$ and NO_2 reached a peak value and decomposed at the same time, leading to the rapid growth of NO and CO. At 2500 K, ∼4 ps, $C_2N_2O_2$, C_2N_2O, and NO_2 all reached the peak value and began to decompose further. Decomposition of C_2N_2O intensified the generation of NO, so the number of NO was the largest among all the products. At 4−8 ps, the decomposition rate of NO_2 was the fastest, which accelerated the generation rate of NO in this stage. The formation rate of NO, after 8 ps, was mainly determined by the further decomposition rate of $C_2N_2O_2$ and C_2N_2O. Similarly, CNO, CO small molecular fragments also became more. At the end of the simulation time, the contents of $C_2N_2O_2$, C_2N_2O, and NO_2 were the least at 2500 K under the three heating conditions, indicating that DNTF molecules decompose more thoroughly. In general, NO_2 is the most active intermediate. The ring cleavage and NO_2 loss are the most important reactions in the initial thermal decomposition of the DNTF supercell. These are consistent with the PE evolution.

Comparing the most frequent reactions and the relative molecular mass (M) of products at the end of the simulation time under the four conditions (Table 6), it can also be found that at T = 1800 K, the cleavage of the central ring caused by O−N (O) bond fracture was the main reaction; at T > 2000 K, NO_2 is the most active intermediate in the whole system. With the increase of temperature, the remaining large molecular fragments decreased and the corresponding small molecular fragments increased. The increase of temperature promotes the further decomposition of large molecule fragments.

Sinditskii et al.[27] mentioned an unknown polymer in their analysis of the thermal decomposition products of DNTF. From the recent work of Lindsey et al.,[32] large $C_xN_yO_z$ species were also observed in the thermal decomposition process of DNTF under extreme conditions, which may be the kinetic precursors to carbon precipitates observed in the experiment, and important information of which needs to be simulated on larger time scales. With the decomposition of DNTF, a large number of small gaseous molecular products are produced, and the system reached the metastable state earlier than other EMs with similar oxygen equilibrium, such as HMX. In our study, species such as $C_xN_yO_z$ also existed at the end of the simulation time, including C_2N_2O and CNO. With the increase of temperature, small gaseous molecules were rapidly produced in large quantities and metastable state appeared, showing poor security. Therefore, more work needs to be done to improve the security of DNTF.

4. CONCLUSIONS

In summary, a series of SCC-DFTB MD simulations were conducted to better understand the thermal decomposition process of DNTF. The initial thermal decomposition pathway of DNTF is strongly dependent on the temperature. At medium and low temperatures such as 1800 K, the O−N (O) bond fracture on the central ring becomes the first and dominant step of the initial thermal decomposition and triggers the cracking of the whole DNTF molecular structure. When T > 2000 K, however, the NO_2 loss on outer ring I is the quickest pathway, which triggers the cleavage of the central ring. High temperatures are more conducive to the formation of small molecular gas products, such as NO and CO. Further chemical reactions of $C_xN_yO_z$ polymers need to be simulated on a larger scale. Much more needs to be done in the future to expand the scope of research to explore the effects of molecular interactions, crystal spatial structure, and charge transfer on HEDMs' thermal decomposition under different conditions.

AUTHOR INFORMATION

Corresponding Author

Yucun Liu − *School of Environment and Safety Engineering, North University of China, Taiyuan 030051, China*; Email: lyc2ct@vip.sina.com

https://doi.org/10.1021/acsomega.1c04166
ACS Omega 2021, 6, 33470−33481

Authors

Yang Li − *School of Environment and Safety Engineering, North University of China, Taiyuan 030051, China;* orcid.org/0000-0002-9063-1994

Junming Yuan − *School of Environment and Safety Engineering, North University of China, Taiyuan 030051, China*

Yiming Luo − *Xi'an Modern Chemistry Research Institute, Xi'an, Shaanxi 710065, China*

Qiuli Jiang − *Xi'an Modern Chemistry Research Institute, Xi'an, Shaanxi 710065, China*

Fanfan Wang − *School of Environment and Safety Engineering, North University of China, Taiyuan 030051, China; Institute of Chemical Materials, China Academy of Engineering Physics (CAEP), Mianyang, Sichuan 621900, China*

Jingwei Meng − *School of Environment and Safety Engineering, North University of China, Taiyuan 030051, China*

Complete contact information is available at: https://pubs.acs.org/10.1021/acsomega.1c04166

Notes

The authors declare no competing financial interest.

■ ACKNOWLEDGMENTS

The research reported was supported by the Open Cooperation and Innovation Fund Project of Xi'an Modern Chemistry Research Institute. The authors gratefully acknowledge the support from the Open Cooperation and Innovation Fund Project of Xi'an Modern Chemistry Research Institute (no. 204J20190387) and the Chaoyang Zhang team.

■ REFERENCES

(1) Zhang, J.; Shreeve, J. n. M. 3,3′-Dinitroamino-4,4′-azoxyfurazan and Its Derivatives: An Assembly of Diverse N-O Building Blocks for High-Performance Energetic Materials. *J. Am. Chem. Soc.* **2014**, *136*, 4437−4445.

(2) Kazakov, A. I.; Dashko, D. V.; Nabatova, A. V.; Stepanov, A. I.; Lempert, D. B. Thermochemical and Energy Characteristics of DNTF and DNFF. *Combust., Explos. Shock Waves* **2018**, *54*, 147−157.

(3) Sheremetev, A. B.; Ivanova, E. A.; Spiridonova, N. P.; Melnikova, S. F.; Tselinsky, I. V.; Suponitsky, K. Y.; Antipin, M. Y. Desilylative nitration ofC,N-disilylated 3-amino-4-methylfurazan. *J. Heterocycl. Chem.* **2005**, *42*, 1237−1242.

(4) Zhou, Y.-S.; Zhang, Z.-Z.; Li, J.-K.; Guan, X.-R.; Huang, X.-P.; Zhou, C. Crystal Structure of 3,4-dinitrofurazanofuroxan. *Chin. J. Explos. Propellants* **2005**, *28*, 43−46.

(5) Li, Y.; Yuan, J. M.; Zhao, W.; Qu, Y.; Xing, X. W.; Meng, J. W.; Liu, Y. C. Application and Development of 3,4-Bis(3-nitrofurazan-4-yl)furoxan (DNTF). *Russ. J. Gen. Chem.* **2021**, *91*, 445−455.

(6) Olofson, R. A.; Michelman, J. S. Furazan*,1,2. *J. Org. Chem.* **1965**, *30*, 1854−1859.

(7) Xue, Q.; Bi, F.; Zhang, J.; Zhang, J.; Wang, B.; Zhang, S. Advances in the Synthesis and Properties of the Isofurazan Energetic Compounds. *Chin. J. Org. Chem.* **2019**, *39*, 1244−1262.

(8) Hu, H.; Zhang, Z.; Zhao, F.; Xiao, C.; Wang, Q.; Yuan, B. A Study on the Properties and Application of High Energy Density Material DNTF. *Acta Armamentarii* **2004**, *25*, 155−158.

(9) Liu, N.; Zeman, S.; Shu, Y.-J.; Wu, Z.-K.; Wang, B.-Z.; Yin, S.-W. Comparative study of melting points of 3,4-bis(3-nitrofurazan-4-yl)furoxan (DNTF)/1,3,3-trinitroazetidine (TNAZ) eutectic compositions using molecular dynamic simulations. *RSC Adv.* **2016**, *6*, 59141−59149.

(10) Ravi, P.; Badgujar, D. M.; Gore, G. M.; Tewari, S. P.; Sikder, A. K. Review on Melt Cast Explosives. *Propellants, Explos., Pyrotech.* **2011**, *36*, 393−403.

(11) Ou, Y. X. *The Science of Explosives*, 1st ed.; Academic Press: Beijing Institute of Technology, 2006; pp 288−291.

(12) Gao, J.; Luo, Y.-M.; Wang, H.; Wang, H.-X.; Wang, W. Risk of Impurities on Thermal Decomposition of DNTF. *Initiators Pyrotech.* **2019**, *3*, 47−50.

(13) Wang, H.; Gao, J.; Tao, J.; Luo, Y.-M.; Jiang, Q.-L. Safety Performances and Molecular Dynamics Simulation of DNTF/HATO. *Chin. J. Energetic Mater.* **2019**, *27*, 897−901.

(14) Wang, H. X.; Gao, J.; Shen, F.; Wang, X. F. Metal Acceleration Ability of a DNAN/DNTF-based Insensitive Explosive. *Explos. Mater.* **2020**, *49*, 21−26.

(15) Zou, Z.; Zhao, F.; Zhang, M.; Tian, J.; Wang, X. Research Progress of 3,4-Dinitrofurazanfuroxan Performances and Its Applications. *Explos. Mater.* **2019**, *48*, 11−16+22.

(16) Feng, X.-J.; Tian, X.; Zhao, J.; Feng, B. Experiment Study on the Influence Factors of the Deflagration to Detonation Transition for DNTF-based Explosives. *Chin. J. Energetic Mater.* **2018**, *26*, 255−259.

(17) Xiong, X.; He, X.; Xiong, Y.; Xue, X.; Yang, H.; Zhang, C. Correlation between the Self-Sustaining Ignition Ability and the Impact Sensitivity of Energetic Materials. *Energ. Mater. Front.* **2020**, *1*, 40−49.

(18) Zhang, C.-Y. On the Energy & Safety Contradiction of Energetic Materials and the Strategy for Developing Low-sensitive High-energetic Materials. *Chin. J. Energetic Mater.* **2018**, *26*, 2−10.

(19) Zhang, C. Origins of the Energy and Safety of Energetic Materials and of the Energy & Safety Contradiction. *Propellants, Explos. Pyrotech.* **2018**, *43*, 855−856.

(20) Sabatini, J.; Oyler, K. Recent Advances in the Synthesis of High Explosive Materials. *Crystals* **2016**, *6*, 5−26.

(21) Badgujar, D.; Talawar, M. B.; Mahulikar, P. P. Review on Promising Insensitive Energetic Materials. *Cent. Eur. J. Energ. Mater.* **2017**, *14*, 821−843.

(22) Gao, H.; Zhao, F.; Qu, W.; Luo, Y. Recent advances in the study of thermodynamic properties and thermokinetic behavior of energetic materials. *Sci. Sin.: Chim.* **2014**, *44*, 953−963.

(23) Feng-qi, Z.; Pei, C.; Rong-zu, H.; Yang, L.; Zhi-zhong, Z.; Yan-shui, Z.; Xu-wu, Y.; Yin, G.; Sheng-li, G.; Qi-zhen, S. Thermochemical properties and non-isothermal decomposition reaction kinetics of 3,4-dinitrofurazanfuroxan (DNTF). *J. Hazard. Mater.* **2004**, *113*, 67−71.

(24) Li, H.-Q.; An, C.-W.; Du, M.-Y.; Wen, X.-M.; Wang, J.-Y. Study on Kinetic Parameters of Thermal Decomposition Reaction and Thermal Stability of 3,4-Bis(3-nitrofurazan-4-yl) furoxan Based on Kissinger Method. *Chin. J. Explos. Propellants* **2016**, *39*, 58−65.

(25) Gao, H.-X.; Zhao, F.-Q.; Hu, R.-Z.; Xu, K.-Z.; Zhang, H.; Wang, P.; Du, Z.-M.; Xu, S.-Y.; Yi, J.-H.; Ma, H.-X.; Chang, C.-R.; Song, J.-R. Specific Heat Capacity, Thermodynamic Properties, Adiabatic Time-to-Explosion and Thermal Sensitivity Probability Density Distribution of 3,4-dinitrofurazanfuroxan (DNTF). *Chem. J. Chin. Univ.* **2008**, *29*, 981−986.

(26) Ren, X.-n.; Wang, J.-n.; Yin, C.-m.; Yu, H.-j.; Heng, S.-y.; Yue, P. Thermal Decomposition Characteristics of a Novel High Energy Density Material DNTF. *Chin. J. Explos. Propellants* **2006**, *29*, 33−36+40.

(27) Sinditskii, V. P.; Burzhava, A. V.; Sheremetev, A. B.; Aleksandrova, N. S. Thermal and Combustion Properties of 3,4-Bis(3-nitrofurazan-4-yl)furoxan (DNTF). *Propellants, Explos., Pyrotech.* **2012**, *37*, 575−580.

(28) Zhang, G.; Jin, S.; Li, L.; Li, Y.; Li, Z.; Wang, D.; Zhang, B.; Jing, B.; Shu, Q. Thermal stability assessment of 3,4-bis(3-nitrofurazan-4-yl)furoxan (DNTF) by accelerating rate calorimeter (ARC). *J. Therm. Anal. Calorim.* **2016**, *126*, 1185−1190.

(29) Tsyshevsky, R.; Kuklja, M. Decomposition Mechanisms and Kinetics of Novel Energetic Molecules BNFF-1 and ANFF-1: Quantum-Chemical Modeling. *Molecules* **2013**, *18*, 8500−8517.

(30) Tsyshevsky, R.; Pagoria, P.; Zhang, M.; Racoveanu, A.; DeHope, A.; Parrish, D.; Kuklja, M. M. Searching for Low-Sensitivity

Cast-Melt High-Energy-Density Materials: Synthesis, Characterization, and Decomposition Kinetics of 3,4-Bis(4-nitro-1,2,5-oxadiazol-3-yl)-1,2,5-oxadiazole-2-oxide. *J. Phys. Chem. C* **2015**, *119*, 3509−3521.
(31) Ju, X.-h.; Ye, C.-c.; Xu, S.-y. Overview on Quantum Chemical Computing and Molecular Dynamic Simulations of Energetic Materials. *Chin. J. Explos. Propellants* **2012**, *35*, 1−8.
(32) Lindsey, R. K.; Bastea, S.; Goldman, N.; Fried, L. E. Investigating 3,4-bis(3-nitrofurazan-4-yl)furoxan detonation with a rapidly tuned density functional tight binding model. *J. Chem. Phys.* **2021**, *154*, 164115−164127.
(33) Wahiduzzaman, M.; Oliveira, A. F.; Philipsen, P.; Zhechkov, L.; van Lenthe, E.; Witek, H. A.; Heine, T. DFTB Parameters for the Periodic Table: Part 1, Electronic Structure. *J. Chem. Theory Comput.* **2013**, *9*, 4006−4017.
(34) Hourahine, B.; Aradi, B.; Blum, V.; Bonafé, F.; Buccheri, A.; Camacho, C.; Cevallos, C.; Deshaye, M. Y.; Dumitrică, T.; Dominguez, A.; Ehlert, S.; Elstner, M.; van der Heide, T.; Hermann, J.; Irle, S.; Kranz, J. J.; Köhler, C.; Kowalczyk, T.; Kubař, T.; Lee, I. S.; Lutsker, V.; Maurer, R. J.; Min, S. K.; Mitchell, I.; Negre, C.; Niehaus, T. A.; Niklasson, A. M. N.; Page, A. J.; Pecchia, A.; Penazzi, G.; Persson, M. P.; Řezáč, J.; Sánchez, C. G.; Sternberg, M.; Stöhr, M.; Stuckenberg, F.; Tkatchenko, A.; Yu, V. W.-z.; Frauenheim, T. DFTB+, a software package for efficient approximate density functional theory based atomistic simulations. *J. Chem. Phys.* **2020**, *152*, 124101−124119.
(35) Aradi, B.; Hourahine, B.; Frauenheim, T. DFTB+, a Sparse Matrix-Based Implementation of the DFTB Method. *J. Phys. Chem. A* **2007**, *111*, 5678−5684.
(36) Zhechkov, L.; Heine, T.; Patchkovskii, S.; Seifert, G.; Duarte, H. A. An Efficient a Posteriori Treatment for Dispersion Interaction in Density-Functional-Based Tight Binding. *J. Chem. Theory Comput.* **2005**, *1*, 841−847.
(37) Jiang, H.; Jiao, Q.; Zhang, C. Early Events When Heating 1,1-Diamino-2,2-dinitroethylene: Self-Consistent Charge Density-Functional Tight-Binding Molecular Dynamics Simulations. *J. Phys. Chem. C* **2018**, *122*, 15125−15132.
(38) Liu, G.; Xiong, Y.; Gou, R.; Zhang, C. Difference in the Thermal Stability of Polymorphic Organic Crystals: A Comparative Study of the Early Events of the Thermal Decay of 2,4,6,8,10,12-Hexanitro-2,4,6,8,10,12-hexaazaisowurtzitane (CL-20) Polymorphs under the Volume Constraint Condition. *J. Phys. Chem. C* **2019**, *123*, 16565−16576.
(39) Berendsen, H. J. C.; Postma, J. P. M.; van Gunsteren, W. F.; DiNola, A.; Haak, J. R. Molecular dynamics with coupling to an external bath. *J. Chem. Phys.* **1984**, *81*, 3684−3690.
(40) Wang, J.; Xiong, Y.; Li, H.; Zhang, C. Reversible Hydrogen Transfer as New Sensitivity Mechanism for Energetic Materials against External Stimuli: A Case of the Insensitive 2,6-Diamino-3,5-dinitropyrazine-1-oxide. *J. Phys. Chem. C* **2018**, *122*, 1109−1118.
(41) Strachan, A.; van Duin, A. C. T.; Chakraborty, D.; Dasgupta, S.; Goddard, W. A., III Shock Waves in High-Energy Materials: The Initial Chemical Events in Nitramine RDX. *Phys. Rev. Lett.* **2003**, *91*, 098301−098304.
(42) Wen, Y.; Zhang, C.; Xue, X.; Long, X. Cluster evolution during the early stages of heating explosives and its relationship to sensitivity: a comparative study of TATB, β-HMX and PETN by molecular reactive force field simulations. *Phys. Chem. Chem. Phys.* **2015**, *17*, 12013−12022.
(43) Zhang, C.; Wen, Y.; Xue, X. Self-Enhanced Catalytic Activities of Functionalized Graphene Sheets in the Combustion of Nitromethane: Molecular Dynamic Simulations by Molecular Reactive Force Field. *ACS Appl. Mater. Interfaces* **2014**, *6*, 12235−12244.
(44) Deng, C.; Liu, J.; Xue, X.; Long, X.; Zhang, C. Coupling Effect of Shock, Heat, and Defect on the Decay of Energetic Materials: A Case of Reactive Molecular Dynamics Simulations on 1,3,5-Trinitro-1,3,5-triazinane. *J. Phys. Chem. C* **2018**, *122*, 27875−27884.
(45) Guo, F.; Cheng, X.-l.; Zhang, H. Reactive Molecular Dynamics Simulation of Solid Nitromethane Impact on (010) Surfaces Induced and Nonimpact Thermal Decomposition. *J. Phys. Chem. A* **2012**, *116*, 3514−3520.
(46) Tsyshevsky, R.; Sharia, O.; Kuklja, M. Molecular Theory of Detonation Initiation: Insight from First Principles Modeling of the Decomposition Mechanisms of Organic Nitro Energetic Materials. *Molecules* **2016**, *21*, 236−257.
(47) Zheng, W.; Wang, J.; Ren, X.; Chen, Z.; Tian, J.; Zhou, Y. Thermal decomposition of 3,4-bis(4′-aminofurazano-3′) furoxan. *J. Hazard. Mater.* **2010**, *177*, 738−742.
(48) Yuan, B.; Bernstein, E. R. Initial mechanisms for the unimolecular decomposition of electronically excited bisfuroxan based energetic materials. *J. Chem. Phys.* **2017**, *146*, 014301−014319.

https://doi.org/10.1021/acsomega.1c04166
ACS Omega 2021, 6, 33470−33481